Supplementary Material for

# Spin current control of magnetism

L. Chen[1], Y. Sun[1], S. Mankovsky[2], T. N. G. Meier[1], M. Kronseder[3], H. Ebert[2], D. Weiss[3] and C. H. Back[1,4,5]

[1]*Department of Physics, Technical University of Munich, Munich, Germany*
[2]*Department of Chemistry, Ludwig Maximilian University, Munich, Germany*
[3]*Institute of Experimental and Applied Physics, University of Regensburg, Regensburg, Germany*
[4]*Munich Center for Quantum Science and Technology, Munich, Germany*
[5]*Center for Quantum Engineering, Technical University of Munich, Munich, Germany*

## Table of Contents:

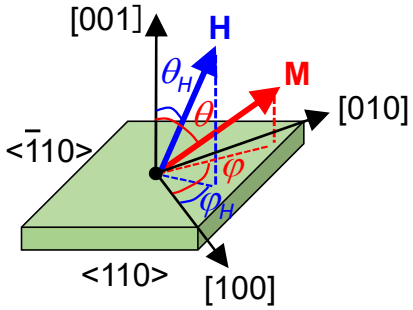


Fig. S1. Schematic of the coordinate system used for the analysis. $\theta_H$ and $\varphi_H$ represent the polar and azimuthal angles of external magnetic-field **H**, and $\theta$ and $\varphi$ are the polar and azimuthal angles of magnetization **M**. The Fe/GaAs thin films show competing in-plane magnetic anisotropies along <100>, <110> and <$\bar{1}$10>-orientations.

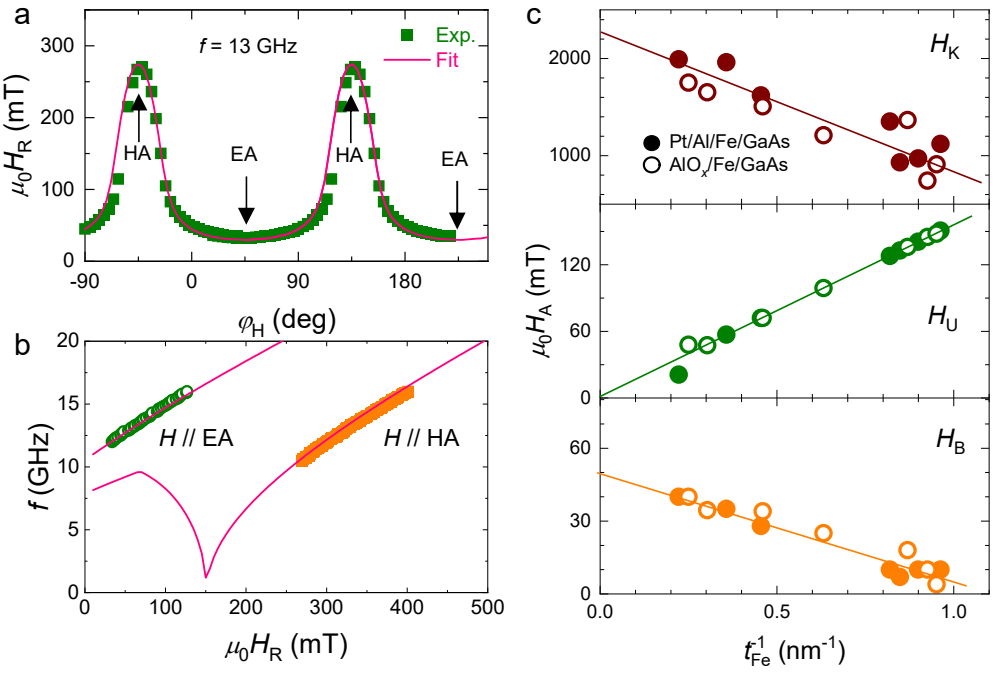


Fig. S2. (**a**) $\varphi_H$ dependence of the resonance field $H_R$ measured for $t_{Fe}$ = 1.2 nm at $f$ = 13 GHz. (**b**) $H_R$ dependence of $f$ measured along the hard axis (HA) and easy axis (EA). In (**a**) and (**b**), the symbols are the experimental data, and the solid lines are the fits by eq. S1. (**c**) Inverse Fe thickness $t_{Fe}^{-1}$ dependence of $H_K$, $H_U$, and $H_B$ for Pt/Al/Fe/GaAs (solid symbols) and AlO$_x$/Fe/GaAs (open symbols). The solids lines are the linear fits.

## Supplementary Note 1: Magnetic anisotropies in Pt/Al/Fe/GaAs multilayers

A typical in-plane magnetic-field angle $\varphi_H$ dependence of the resonance field $H_R$ for $t_{Fe}$ = 1.2 nm measured at $f$ = 13 GHz is shown in Fig. S2a. The sample shows typical in-plane uniaxial anisotropy with two-fold symmetry, i.e., a magnetically hard axis (HA) for $\varphi_H$ = –45° and 135° (<$\bar{1}$10>-orientations) and a magnetically easy axis (EA) for $\varphi_H$ = 45° and 225° (<110>-orientations), which originates from the anisotropic bonding at the Fe/GaAs interface. To quantify the magnitude of the anisotropies, we further measure the $f$ dependence of $H_R$ both along the EA and the HA (Fig. S2b). Both the angular- and frequency-dependence of $H_R$ are fitted according to[S1,S2]

$$\left(\frac{2\pi f}{\gamma}\right)^2 = \mu_0^2 H_1^R H_2^R, \tag{S1}$$

with $H_1^R = H^R\cos(\varphi - \varphi_H) + H_K + H_B(3 + \cos4\varphi)/4 - H_U\sin^2(\varphi - 45°)$, and $H_2^R = H^R\cos(\varphi - \varphi_H) + H_B\cos4\varphi - H_U\sin2\varphi$. Here, $\gamma (= g\mu_B/\hbar)$ is the gyromagnetic ratio, $g$ the Landé $g$-factor, $\mu_B$ the Bohr magneton, $\hbar$ the reduced Planck constant. $H_K$ $(= M - H_\perp)$ the effective demagnetization magnetic anisotropy field including the perpendicular magnetic anisotropy field $H_\perp$, $H_B$ the biaxial magnetic anisotropy field along <100> orientations, $H_U$ the in-plane uniaxial magnetic anisotropy field along <110> orientations, and $\varphi$ the in-plane angle of magnetization as defined in Fig. S1. The magnitude of $\varphi$ is obtained by the equilibrium condition

$$H_R\sin(\varphi - \varphi_H) + (H_B/4)\sin4\varphi + (H_U/2)\cos2\varphi = 0. \tag{S2}$$

It can be checked that $\varphi = \varphi_H$ holds when **H** is along <110>- and <$\bar{1}$10>-orientations. From the fits of $H_R$, the magnitude of the magnetic anisotropy fields $H_A$ ($H_A = H_K, H_B, H_U$) for each $t_{Fe}$ is obtained, and their dependences on inverse Fe thickness $t_{Fe}^{-1}$, together with the results obtained from the $AlO_x$/Fe/GaAs samples, are summarized in Fig. S2c. The results show that the Pt/Al/Fe/GaAs samples

have virtually identical magnetic anisotropies as the $AlO_x$/Fe/GaAs samples, and introducing the Pt/Al layer neither enhances the magnetization leading to an increase of $H_K$ nor generates a perpendicular anisotropy leading to a decrease of $H_K$. For both sample series, $H_K$ and $H_B$ decrease as $t_{Fe}$ decreases due to the reduction of the magnetization as $t_{Fe}$ decreases, and both of them scale linearly with $t_{Fe}^{-1}$. The intercept (~2220 mT) of the $H_K$ - $t_{Fe}^{-1}$ trace corresponds to the saturation magnetization of bulk Fe, and the intercept (~45 mT) of the $H_B$ - $t_{Fe}^{-1}$ trace corresponds to the biaxial anisotropy of bulk Fe. In contrast to $H_K$ and $H_B$, $H_U$ shows a linear dependence on $t_{Fe}^{-1}$ with a zero intercept, indicative of the interfacial origin of $H_U$.

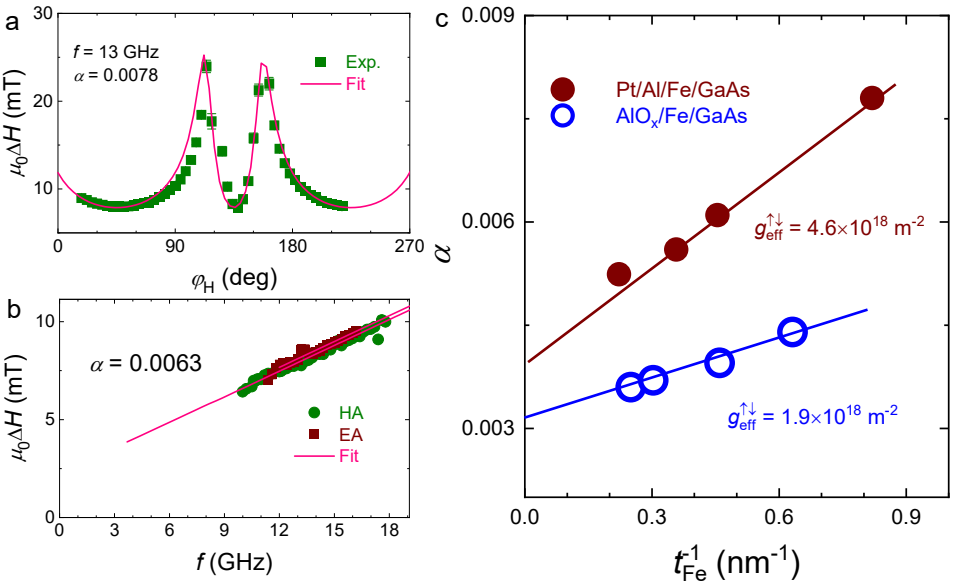


Fig. S3. (**a**) $\varphi_H$ dependence of $\Delta H$ for $t_{Fe}$ = 1.2 nm measured at $f$ = 13 GHz. The solid line is fitted using a damping value of 0.0078. (**b**) $f$ dependence of $\Delta H$ measured along the EA and HA. The solid lines are the fits by a damping value of 0.0063. (**c**) $t_{Fe}^{-1}$ dependence of $\alpha$ for Pt/Al/Fe/GaAs samples (solid symbols) as well as $AlO_x$/Fe/GaAs samples (open symbols). The solid lines are the fits according to spin pumping.

## Supplementary Note 2: Effective mixing conductance in Pt/Al/Fe/GaAs multilayers

Figs. S3a and b respectively show the $\varphi_H$-dependence and $f$-dependence of linewidth $\Delta H$ for $t_{Fe}$ = 1.2 nm. The magnitude of $\Delta H$ varies strongly with $\varphi_H$ due to the presence of in-plane anisotropy and the dependencies of $\Delta H$ on $f$ along both EA and HA show linear behaviour. Both the angular and frequency dependence of $\Delta H$ can be well fitted by[S3],

$$\Delta H = \Delta[\mathrm{Im}(\chi)] + \Delta H_0 = \Delta\left[\frac{\alpha\sqrt{H_1^R H_2^R}(H_1 H_1 + H_1^R H_2^R)M}{(H_1 H_2 - H_1^R H_2^R)^2 + \alpha^2 H_1^R H_2^R (H_1 + H_2)^2}\right] + \Delta H_0, \quad \text{(S3)}$$

where $\Delta[\mathrm{Im}(\chi)]$ is the linewidth of the imaginary part of the dynamic magnetic susceptibility $\mathrm{Im}(\chi)$, $H_1$ and $H_2$ are defined in eq. S1 for arbitrary $H$ values, and $\Delta H_0$ is the residual linewidth (zero-frequency intercept). Since the angular trace can be well fitted by using a damping value of 0.0078, there is no need to consider other extrinsic effects (i.e., inhomogeneity and/or two-magnon scattering) contributing to $\Delta H$. It is worth mentioning that the angular trace gives a slightly higher $\alpha$ value because $\Delta H_0$, which also depends on $\varphi_H$, is not considered in the fit. In this case, the frequency dependence of linewidth gives more reliable damping values (as shown in Fig. S3b). Fig. S3c compares the magnitude of damping for Pt/Al/Fe/GaAs and $AlO_x$/Fe/GaAs samples. For both sample series, the Gilbert damping increases as $t_{Fe}$ decreases and a linear dependence of $\alpha$ on $t_{Fe}^{-1}$ is observed. The enhancement of $\alpha$ is due to the spin pumping effect, which is given by[S4,S5]

$$\alpha = \alpha_0 + g_{\mathrm{eff}}^{\uparrow\downarrow}\frac{\gamma\hbar}{4\pi M}t_{\mathrm{Fe}}^{-1}, \quad \text{(S4)}$$

where $\alpha_0$ is the intrinsic damping of pure bulk Fe, and $g_{\mathrm{eff}}^{\uparrow\downarrow}$ the effective spin mixing conductance quantifying the spin pumping efficiency. By using $\mu_0 M$ = 2.2 T and $\gamma$ = 1.80×10$^{11}$ rad.s$^{-1}$T$^{-1}$, the

magnitude of $g_{\mathrm{eff}}^{\uparrow\downarrow}$ for Pt/Al/Fe/GaAs is determined to be $4.6\times10^{18}$ $\mathrm{m}^{-2}$, and $g_{\mathrm{eff}}^{\uparrow\downarrow}$ at the Fe/GaAs interface is determined to be $1.9\times10^{18}$ $\mathrm{m}^{-2}$. Therefore, by subtracting these two values, the magnitude of $g_{\mathrm{eff}}^{\uparrow\downarrow}$ at Pt/Al/Fe interface is determined to be $2.7\times10^{18}$ $\mathrm{m}^{-2}$. The spin transparency $T_{\mathrm{int}}$ of the Pt/Al/Fe interface is given by[S5]

$$T_{\mathrm{int}}=\frac{2e^2}{h}\frac{g_{\mathrm{eff}}^{\uparrow\downarrow}}{G_{\mathrm{Pt}}} \tag{S5}$$

where $\frac{2e^2}{h}$ is the conductance quantum, $G_{\mathrm{Pt}}$ [$= 1/(\rho_{xx}\lambda_{\mathrm{s}})$] the spin conductance of Pt, $\rho_{xx}$ the resistivity, and $\lambda_{\mathrm{s}}$ the spin diffusion length. By using $\lambda_{\mathrm{s}} = 4$ nm and an averaged $\rho_{xx} = 40$ μΩcm, $T_{\mathrm{int}} = 0.21$ is determined. We notice that the magnitude of $g_{\mathrm{eff}}^{\uparrow\downarrow}$ at the Pt/Al/Fe interface is about one order of magnitude smaller than the experimental values found at heavy metal/ultra-thin ferromagnet interfaces[S6], but very close to the value obtained by first principle calculations[S7]. The previously overestimated $g_{\mathrm{eff}}^{\uparrow\downarrow}$ and thus $T_{\mathrm{int}}$ at heavy metal/ultra-thin ferromagnet interfaces is probably due to the fact that the enhancement of $\alpha$ by two-magnon scattering is not properly excluded[S8]. Moreover, the obtained $\alpha_0$ values for Pt/Al/Fe/GaAs ($\alpha_0 = 0.0039$) and $\mathrm{AlO}_x$/Fe/GaAs ($\alpha_0 = 0.0033$) slightly differ; the reason is unclear to us, but might be due to a small error in the Fe thickness, which is hard to be determined accurately in the ultrathin regime.

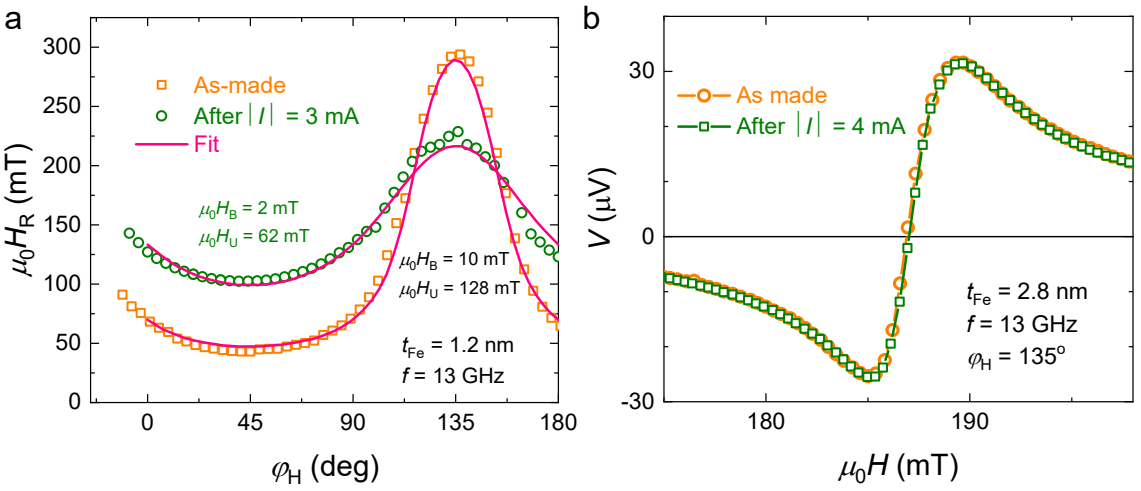


Fig. S4. (**a**) $\varphi_H$ dependence of $H_R$ of $t_{Fe}$ = 1.2 nm measured in the as-fabricated state and after applying |*I*| of 3 mA. The application of the relatively large current partially destroys the magnetic properties, i.e., the uniaxial anisotropy decreases from 128 mT to 62 mT and the biaxial anisotropy decreases from 10 mT to 2 mT. (**b**) FMR spectra measured in the as-fabricated state and after applying a dc current |*I*| of 4 mA for $t_{Fe}$ of 2.8 nm. The FMR spectrum remains unchanged after the application of the dc current.

| $t_{Fe}$ (nm) | 4.5 | 2.8 | 2.2 | 1.2 | 1.1 |
|---|---|---|---|---|---|
| $\|I_{opt}\|$ (mA) | 4.5 | 4 | 4 | 1.5 | 1.5 |

Table S1. Optimal current applied for each Fe thickness without detrimental effect by Joule heating.

## Supplementary Note 3: Ruling out possible detrimental effects arising from the application of a dc current

To observe the modification of magnetic anisotropies and Gilbert damping, sizeable charge currents are needed. The application of charge currents inevitably generates Joule heating, and could partially and/or completely damage the device. Figure S4a shows an example for the case that applying a relatively large current of 3 mA significantly reduces the uniaxial magnetic anisotropy from 128 mT to 62 mT, and reduces the biaxial anisotropy from 10 mT to 2 mT for $t_{Fe}$ = 1.2 nm. In

this case, the change of magnetic properties is irreversible since the device is partially damaged probably due to interdiffusion. To rule out the possibility that the current-induced modification is not due to any detrimental effect by Joule heating, we increase the magnitude of the current step-by-step, and measured the FMR spectra before and after applying the dc current. An optimal current value $|I_{opt}|$ is determined by two criteria: I) it shows sizeable modification of the linewidth and the resonance field, and II) the FMR spectra should be identical before and after applying the optimal charge current. An example is shown in Fig. S4b for $t_{Fe}$ = 2.8 nm. According to our expertise, although the device sizes (4 μm × 20 μm) and the Pt (6 nm)/Al (1.5 nm) layer thicknesses are identical, the optimal current for each $t_{Fe}$ differs. As summarized in Table S1, the thinner the $t_{Fe}$, the lower the $|I_{opt}|$ is.

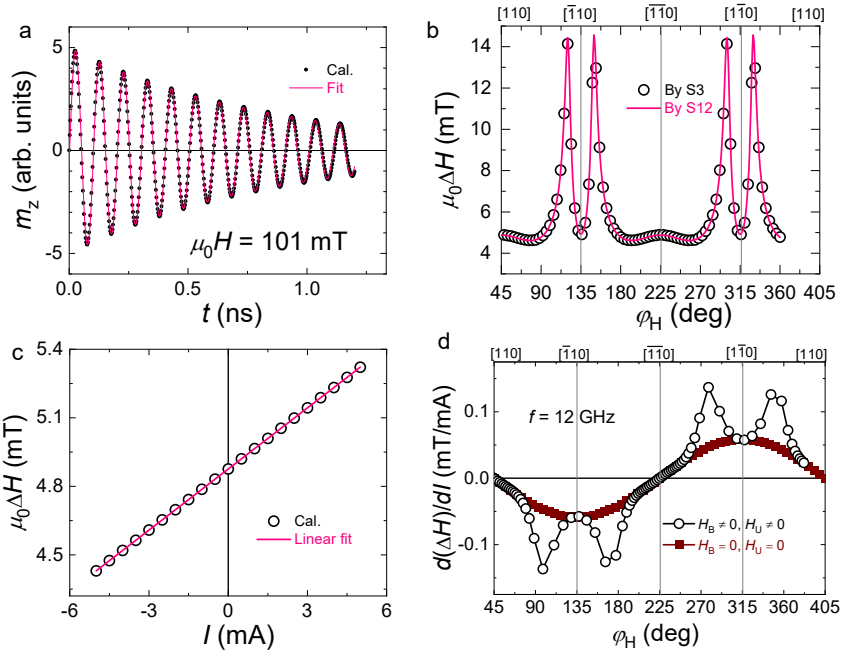


Fig. S5. (**a**) Time-resolved dynamic magnetization calculated by eq. S9 for $\mu_0 H$ = 101 mT. By fitting the damped oscillation of the dynamic magnetization (solid line) by eq. S11, the magnetization relaxation time is obtained. (**b**) Calculated $\varphi_H$ dependence of $\Delta H$ by eq. S3 and eq. S12 using $\alpha$ = 0.0063. Both methods show identical results. (**c**) Calculated $I$-dependence of $\Delta H$; the solid line is the linear fit from which $d(\Delta H)/dI$ is obtained. (**d**) Comparison of the $\varphi_H$ dependence of $d(\Delta H)/dI$ calculated with in-plane anisotropy (open symbols) and without in-plane anisotropies (solid symbols).

## Supplementary Note 4: Theory of the modulation of the linewidth by spin Hall effect

To model the modulation of the FMR linewidth by the application of dc current, the Landau-Lifshitz-Gilbert equation with damping-like spin-torque term should be considered[S9],

$$\frac{d\mathbf{M}}{dt} = -\gamma\mathbf{M}\times\mu_0\mathbf{H}_{\text{eff}} + \frac{\alpha}{M}\mathbf{M}\times\frac{\mathrm{d}\mathbf{M}}{\mathrm{d}t} - \frac{\gamma\mu_0 h_{\text{DL}}}{M}\mathbf{M}\times\mathbf{M}\times\boldsymbol{\sigma}. \tag{S6}$$

The terms on the right side of eq. S6 respectively correspond to the precession torque, the damping torque and the damping-like spin-torque induced by the spin Hall effect. Here $\boldsymbol{\sigma}$ is the spin polarization unit vector, and $h_{\text{DL}}$ is the effective anti-damping-like magnetic-field. The effective magnetic field $\mathbf{H}_{\text{eff}}$, containing both external and internal fields, is expressed in terms of the free energy density $F$, which can be obtained as

$$\mathbf{H}_{\text{eff}} = -\frac{1}{\mu_0}\frac{\partial F}{\partial \mathbf{M}} \tag{S7}$$

For single crystalline Fe films grown on GaAs (001) substrates with in-plane magnetic anisotropies, $F$ is given by

$$F = \frac{\mu_0 M}{2}\left\{-2H\left[\cos\theta\cos\theta_{\text{H}} + \sin\theta\sin\theta_{\text{H}}\cos(\varphi-\varphi_{\text{H}})\right] + H_{\text{K}}\cos^2\theta - \frac{H_{\text{B}}}{2}\sin^4\theta\frac{3+\cos 4\varphi}{4} - H_{\text{U}}\sin^2\theta\sin^2\left(\varphi-\frac{\pi}{4}\right)\right\}. \tag{S8}$$

Bringing eqs. S7 and S8 into eq. S6, the time-resolved magnetization dynamics for current flowing along the [110]-orientation (i.e., $\boldsymbol{\sigma}$ // $[\bar{1}10]$) is obtained as

$$\begin{cases} \frac{\partial\varphi}{\partial t} = \frac{\gamma\mu_0}{(1+\alpha^2)M\sin\theta}\left(\frac{\partial F}{\partial\theta} - \frac{\alpha}{\sin\theta}\frac{\partial F}{\partial\varphi}\right) + \frac{\gamma\mu_0 h_{DL}}{(1+\alpha^2)\sin\theta}\frac{\sqrt{2}}{2}\left[\alpha\cos\theta\,(\sin\varphi-\cos\varphi)+\cos\varphi+\sin\varphi\right] \\ \frac{\partial\theta}{\partial t} = \frac{\gamma\mu_0}{M\sin\theta}\left(\frac{\alpha^2}{1+\alpha^2}-1\right)\frac{\partial F}{\partial\varphi} - \frac{\alpha}{1+\alpha^2}\frac{\gamma\mu_0}{M}\frac{\partial F}{\partial\theta} + \left(1+\frac{\alpha^2}{1+\alpha^2}\right)\gamma\mu_0 h_{DL}\frac{\sqrt{2}}{2}\cos\theta\,(\sin\varphi-\cos\varphi) + \frac{\alpha}{1+\alpha^2}\gamma\mu_0 h_{DL}\frac{\sqrt{2}}{2}(\cos\varphi+\sin\varphi) \end{cases} \tag{S9}$$

Similarly, for the current flowing along the [100]-orientation (i.e., $\boldsymbol{\sigma}$ // [010]), we have

$$\begin{cases} \frac{\partial\varphi}{\partial t} = \frac{\gamma\mu_0}{(1+\alpha^2)M\sin\theta}\left(\frac{\partial F}{\partial\theta} - \frac{\alpha}{\sin\theta}\frac{\partial F}{\partial\varphi}\right) + \frac{\gamma\mu_0 h_{DL}}{(1+\alpha^2)\sin\theta}\left(\alpha\cos\theta\sin\varphi+\cos\varphi\right) \\ \frac{\partial\theta}{\partial t} = \frac{\gamma\mu_0}{M\sin\theta}\left(\frac{\alpha^2}{1+\alpha^2}-1\right)\frac{\partial F}{\partial\varphi} - \frac{\alpha}{1+\alpha^2}\frac{\gamma\mu_0}{M}\frac{\partial F}{\partial\theta} - \gamma\mu_0 h_{DL}\left[\frac{\alpha^2}{1+\alpha^2}\left(\alpha\cos\theta\sin\varphi+\cos\varphi\right) - \cos\theta\sin\varphi\right] \end{cases} \tag{S10}$$

The time dependence of $\varphi(t)$, $\theta(t)$ and then $\mathbf{m}(t)$ can be readily obtained from eqs. S9 and S10, and

Fig. S5a shows an example of the time dependent $m_z$ by using $\mu_0 H$ = 101 mT, $\mu_0 H_K$ = 1350 mT, $\mu_0 H_U$ = 128 mT, $\mu_0 H_B$ = 10 mT, $\alpha$ = 0.0063 and $\mu_0 H_{DL}$ = 0. The damped oscillating dynamic magnetization can be well fitted by

$$m_z(t) = Ae^{-t/\tau}\cos(2\pi ft+\phi) \tag{S11}$$

where $A$ is the amplitude, $\tau$ the magnetization relaxation time, and $\phi$ the phase shift. The connection between $\tau$ and $\Delta H$ is given by

$$\Delta H = \frac{1}{2\pi}\left|\frac{dH_R}{df}\right|\frac{1}{\tau} \tag{S12}$$

where $\frac{dH_R}{df}$ can be readily obtained from Eq. S1. We confirm the validity of the above method in Fig. S5b by showing that the angular dependence of $\Delta H$ obtained from the time domain (eq. S12) at $h_{DL}$ = 0 is identical to the linewidth obtained by the dynamic susceptibility in magnetic-field domain (eq. S3).

Having obtained the linewidth for $I$ = 0, the next step is to calculate the influence of the linewidth by spin-orbit torque. The magnitude of $h_{DL}$ is given by

$$\mu_0 h_{DL} = \frac{\hbar}{2e}\frac{\xi}{Mt_{Fe}} j_{Pt} \tag{S13}$$

where $\xi$ ισ the effective damping-like torque efficiency, and $j_{Pt}$ the current density in Pt. For the Pt/Al/Fe multilayer, $j_P$ is determined by the parallel resistor model

$$j_{Pt} = \frac{t_{Pt}\rho_{Al}\rho_{Fe}}{t_{Pt}\rho_{Al}\rho_{Fe}+t_{Al}\rho_{Pt}\rho_{Fe}+t_{Fe}\rho_{Pt}\rho_{Al}} \cdot \frac{I}{wt_{Pt}} \tag{S14}$$

where $\rho_{Pt}$ (= 40 μΩ.cm), $\rho_{Al}$(= 10 μΩ.cm), $\rho_{Fe}$(= 50 μΩ.cm) are the resistivities of the Pt, Al, and Fe layers, $t_{Pt}$, $t_{Al}$ $t_{Fe}$ the thicknesses of the Pt, Al, Fe layers, $I$ the dc current, and $w$ the width of the device.

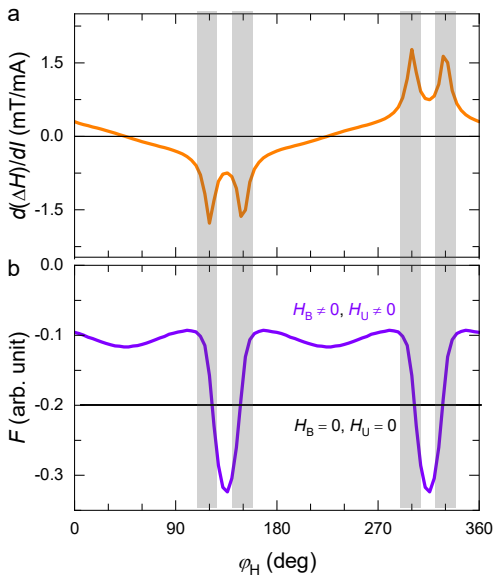


Fig. S6. $\varphi_H$ dependence of the calculated modulation of linewidth $d(\Delta H)/dI$ (**a**), and free energy $F$ (**b**). Around the HA (shaded areas), the energy barrier vanishes and all the static torques acting on **M** cancel out. In this case, the magnetization has a larger precessional cone angle, leading to an enhanced modulation of damping.

Plugging eqs. S13 and S14 into eqs. S9 and S10, the $I$-dependence of $\Delta H$ can be obtained. An example is displayed in Fig. S5c, which shows a linear $\Delta H$–$I$ relationship. From the linear fit (Eq. 1 in the main text), one obtains the modulation amplitude of $\Delta H$, i.e., $d(\Delta H)/dI$. Fig. S5d presents the calculated $d(\Delta H)/dI$ as a function of magnetic-field angle, which shows a strong variation around the hard axis.

To reproduce the experimental data as shown in Fig. 1f in the main text, the magnitude of the magnetic anisotropies and the damping parameter obtained in Fig. S2 as well as $\xi = 0.06$ are used. If the in-plane anisotropy is turned off, the angular trace shows simply a $\sin\varphi$ dependence, which has been experimentally verified by in polycrystalline Pt/Py bi-layers[S10,S11].

To understand the strong deviation of $d(\Delta H)/dI$ around the hard axis, we plot the in-plane angular dependence of $F$ in Fig. S6 for $\theta = \theta_H = 90^o$, i.e.,

$$F = \frac{\mu_0 M}{2}\left[-2H_R\cos(\varphi-\varphi_H) - \frac{H_B}{2}\frac{3+\cos 4\varphi}{4} - H_U\sin^2\left(\varphi-\frac{\pi}{4}\right)\right]. \quad \text{(S15)}$$

It shows that, around the hard axis (~ ±15°), the magnetic potential barrier completely vanishes and $\frac{\partial F}{\partial \varphi_H} = 0$ & $\frac{\partial^2 F}{\partial \varphi_H^2} < 0$ holds. This indicates that the net static torques induced by internal and external magnetic-fields acting on the magnetization cancel out and the magnetization has a large cone angle for precession[S12]. The low stiffness around the hard axis allows larger $d(\Delta H)/dI$ values induced by SHE[S13]. If there are no in-plane magnetic anisotropies, the free energy is constant and independent of the angle, the magnetization always follows the direction of the applied magnetic-field and has the same stiffness at each position. Therefore, the modulation shows no deviation around the hard axis.

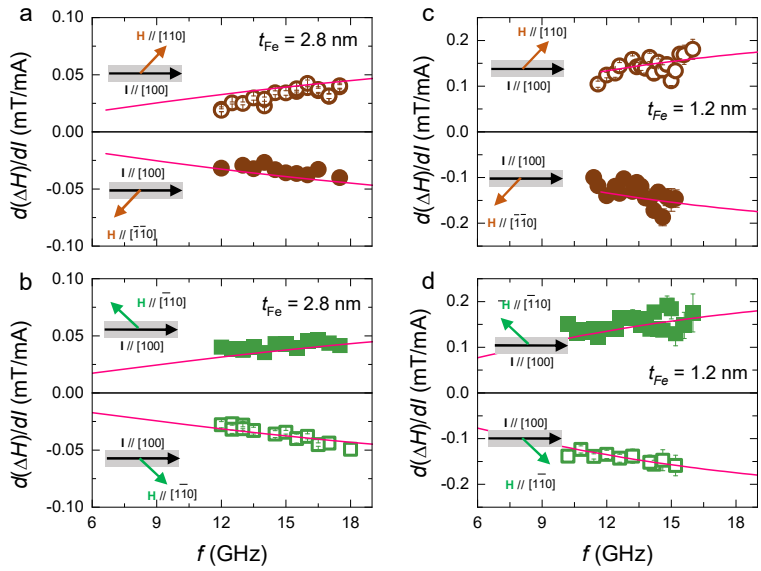


Fig. S7. (**a**) Frequency dependence of $d(\Delta H)/dI$ for $H$ along the easy axis ([110]- and [$\bar{1}\bar{1}$0]-orientations). (**b**) Frequency dependence of $d(\Delta H)/dI$ for $H$ along the hard axis ([$\bar{1}$10]- and [1$\bar{1}$0]-orientations). The results in (**a**) and (**b**) are obtained for $t_{Fe}$ = 2.8 nm. (**c**) and (**d**) are the same results as (**a**) and (**b**) but for $t_{Fe}$ = 1.2 nm. The inset of each figures shows the respective orientation of the charge current and magnetic-field (magnetization). The solid lines in each panel are calculated by eq. S10 using $\xi$ = 0.06.

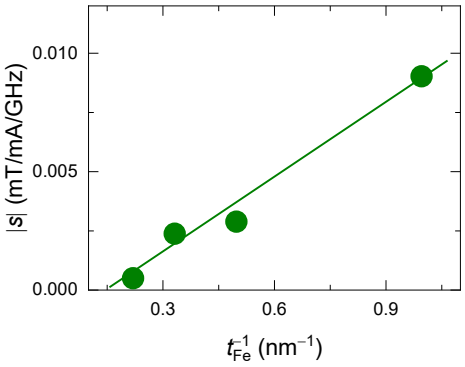


Fig. S8. $t_{Fe}^{-1}$ dependence of |s| extracted from Fig. S7, where $s = \frac{d[d(\Delta H)/dI]}{df}$.

## Supplementary Note 5: Frequency dependence of the linewidth modulation

Fig. S7a shows the frequency dependence of the modulation of linewidth $d(\Delta H)/dI$ for $t_{Fe}$ = 2.8 nm and 1.2 nm, where the current flows along [100]. For both samples, the modulation changes polarity as the direction of **M** is changed by 180°. The modulation amplitude increases quasi-linearly with frequency, and the experimental results can be also reproduced by eq. S10 using $\xi$= 0.06, consistent with angular modulation shown in Fig. 2f. For **H** along <110>- and <$\bar{1}$10>-orientations, the frequency and the Fe thickness dependence of linewidth modulation is approximately given by[S14]

$$\frac{d(\mu_0 \Delta H)}{d(I)} = 2\frac{2\pi f}{\gamma}\frac{\sin\varphi_{I-H}}{H_R + H_K/2}\frac{\hbar}{2e}\frac{\xi}{Mt_{Fe}}\frac{1}{t_{Pt}w}, \quad \text{(S16)}$$

where $\varphi_{I\text{-}H}$ = 45°, 135°, 225°, and 315° as shown by the inset of each figure. The damping-like torque efficiency can be quantified by the slope $s$ of $f$-dependence modulation, i.e., $s = \frac{d[d(\Delta H)/dI]}{df}$. Figure S8 shows the absolute value of $s$ values as function of $t_{Fe}^{-1}$. A linear dependence of $|s|$ on $t_{Fe}^{-1}$ is observed, which indicates that the damping-like torque is an interfacial effect, originating from the absorption of spin generated by the spin Hall effect in Pt[S15].

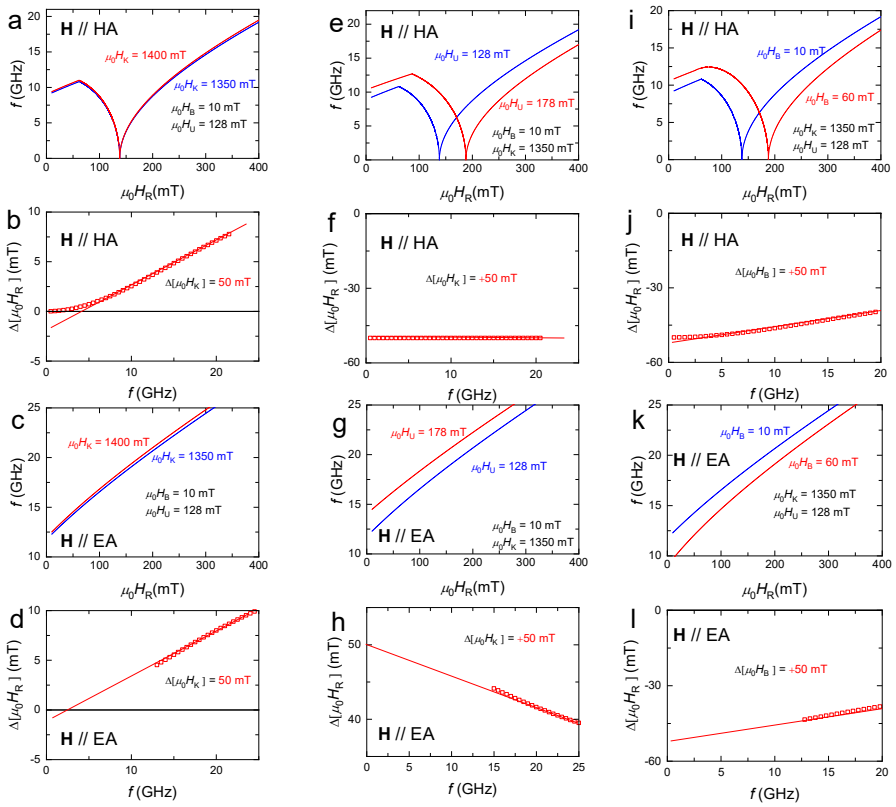


Fig. S9. (**a**) $H_R$-dependence of $f$ calculated for $\mu_0 H_K$ = 1350 mT (blue) and $\mu_0 H_K + \mu_0 \Delta H_K$ = 1400 mT (red) along the hard axis. (**b**) Shift of the resonance field $\Delta H_R$ as a function of frequency, where $\Delta H_R = H_R(H_K) - H_R(H_K + \Delta H_K)$. (**c**) and (**d**) are the same results as shown in (**a**) and (**b**) but for the calculation along the easy axis. (**e**)-(**h**) and same as Figs. (**a**)-(**d**) but for $\Delta H_U$. (**i**)-(**l**) for $\Delta H_B$. In the calculation, a change of magnetic anisotropy fields of 50 mT is assumed for each case to exaggerate the shift of $H_R$.

| Axis | $\Delta H_K$ | $\Delta H_B$ | $\Delta H_U$ |
|---|---|---|---|
| EA | $\Delta H_R = k_K f$ | $\Delta H_R = -\Delta H_B + k_B f$ | $\Delta H_R = \Delta H_U - k_U f$ |
| HA | $\Delta H_R = k_K f$ | $\Delta H_R = -\Delta H_B + k_B f$ | $\Delta H_R = -\Delta H_U$ |

Table S2. Summary of the $\Delta H_R$-$f$ relationships induced by the change of $H_K$, the change of $H_B$, and the change of $H_U$. Here the slope $k$ ($k$ = $k_K$, $k_U$, $k_B$) is the slope quantifying the modulation induced by the change of anisotropy $\Delta H_A$ ($\Delta H_A$ = $\Delta H_K$, $\Delta H_B$, $\Delta H_U$). For $\Delta H_R$ induced by $\Delta H_K$ and $\Delta H_B$, $k \propto \Delta H_A$, which holds for both EA and HA. While for $\Delta H_R$ induced by $\Delta H_U$, $k \propto -\Delta H_U$, which holds only for EA.

## Supplementary Note 6: Quantifying the modification of the magnetic anisotropies by spin currents

In this section, we show our procedure to quantify the modulation of magnetic anisotropies by spin currents. According to eq. S1, the $f$-dependencies of $H_R$ along the easy axis ($\varphi_H = \varphi = 45^o$ and $225^o$) and the hard axis ($\varphi_H = \varphi = 135^o$ and $315^o$) are given by[S1,S2]

$$\begin{cases} \left(\frac{2\pi f}{\gamma}\right)^2 = \mu_0^2 \left(H_R^{EA} + H_K + \frac{H_B}{2}\right)\left(H_R^{EA} - H_B - H_U\right) \\ \left(\frac{2\pi f}{\gamma}\right)^2 = \mu_0^2 \left(H_R^{HA} + H_K + \frac{H_B}{2} - H_U\right)\left(H_R^{HA} - H_B + H_U\right) \end{cases}. \quad \text{(S17)}$$

From the angular and frequency dependence of $H_R$ as shown in Fig. S2, $\mu_0 H_K$ = 1350 mT, $\mu_0 H_U$ = 128 mT, $\mu_0 H_B$ = 10 mT and $g$ = 2.05 are determined for $t_{Fe}$ = 1.2 nm. Figure S8a shows the $H_R$ dependence of $f$ for $\mu_0 H_K$ = 1350 mT (blue solid line) and $\mu_0 H_K + \Delta\mu_0 H_K$ = 1400 mT (red solid line) along the hard axis calculated by eq. S16. To exaggerate the difference, $\mu_0 \Delta H_K$ of 50 mT is assumed. The shift of the resonance field $\Delta H_R$ is obtained as $\Delta H_R = H_R(H_K) - H_R(H_K + \Delta H_K)$, and the frequency dependence of $\Delta H_R$ is plotted in Fig. S8b, which shows a linear behavior with respect to $f$ between 10 GHz and 20 GHz (in the experimental range), i.e., $\Delta H_R = k_K f$. Note that, to simplify the analysis, the zero-frequency intercept is ignored since the magnitude is much smaller than the intercept induced by $\Delta H_U$ and $\Delta H_B$. The sign of the slope $k_K$ is the same as $\Delta H_K$ and its magnitude is proportional to $\Delta H_K$, i.e., $k_k \propto \Delta H_K$. For the easy axis as shown in Figs. S8c and d, the $\Delta H_R$-$f$ relationship induced by $\Delta H_K$ remains the same as for the hard axis, i.e., $\Delta H_R = k_K f$ still holds.

Figure S8e shows the $H_R$-dependence of $f$ for $\mu_0 H_U$ = 128 mT (blue solid line) and $\mu_0 H_U + \mu_0 \Delta H_U$ = 178 mT (red solid line) along the hard axis. As shown in Fig. S8f, the shift of the resonance field along the hard axis is independent of $f$, i.e., $\Delta H_R = -\Delta H_U$. However, for the easy axis as shown in

Figs. S8g and h, the *f*-dependent $\Delta H_R$ can be expressed as $\Delta H_R = \Delta H_U - k_U f$, which has an opposite slope compared to the $\Delta H_R$-*f* relationships induced by $\Delta H_K$ (Fig. S8d), i.e., $k_U \propto -\Delta H_U$.

If the modulation is induced by a change of the biaxial anisotropy as shown in Figures S7i-l, $\Delta H_R$ along both the hard and easy axis shows a linear dependence on *f*, which is be expressed as $\Delta H_R = -\Delta H_B - k_B f$, and $k_B \propto \Delta H_B$ holds.

Table summarizes the $\Delta H_R$-*f* relationships both along the easy and hard axes induced by the change of $H_K$, the change of $H_B$, and the change of $H_U$.

Since $h_{Oe/FL}$ generated by the dc current also shifts the resonance field along the EA and HA axes by $\pm\frac{\sqrt{2}}{2}h_{Oe/FL}$, where '+' corresponds to the [110] (easy axis) and the $[\bar{1}10]$ (hard axis) directions, and '–' corresponds to the $[\bar{1}\bar{1}0]$ (easy axis) and the $[1\bar{1}0]$ (hard axis) directions, the total $\Delta H_R$ induced by $\Delta H_K$ $\Delta H_U$ and $\Delta H_B$ along the easy and hard axes is respectively obtained as

$$\Delta H_R^{EA}(f) = \Delta H_U - \Delta H_B \pm \frac{\sqrt{2}}{2}h_{Oe/FL} + (k_K + k_B - k_U)f \quad \text{(S18)}$$

$$\Delta H_R^{HA}(f) = -(\Delta H_U + \Delta H_B) \pm \frac{\sqrt{2}}{2}h_{Oe/FL} + (k_K + k_B)f \quad \text{(S19)}$$

Based on eqs. S18 and S19, the values of $\Delta H_K$ $\Delta H_U$, $\Delta H_B$ and $h_{Oe/FL}$ for $t_{Fe} \leq 2.2$ nm are extracted as follows:

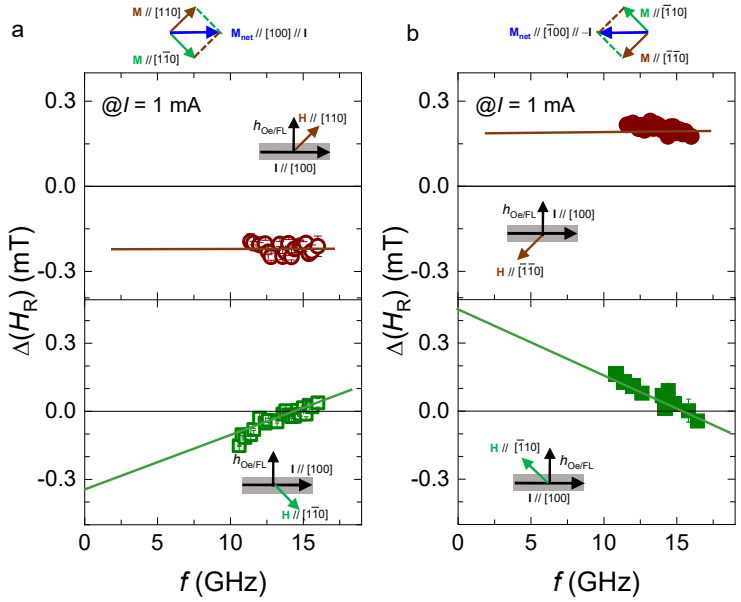


Fig. S10. (**a**) Shift of the resonance field $\Delta H_R$ for $I$ = 1 mA for **H** // **M** // [$\bar{1}\bar{1}$0] (easy axis) and **H** // **M** // [1$\bar{1}$0] (hard axis) for $t_{Fe}$ = 1.2 nm. (**b**) Shift of the resonance field for $I$ = 1 mA for **H** // **M** // [110] (easy axis) and **H** // **M** // [$\bar{1}$10] (hard axis) for the same sample. The inset in each figure shows the orientation of **H** with respect to the current. The upper panel of each figure shows the net magnetization, which is parallel to **I** (**a**) and anti-parallel to **I** (**b**).

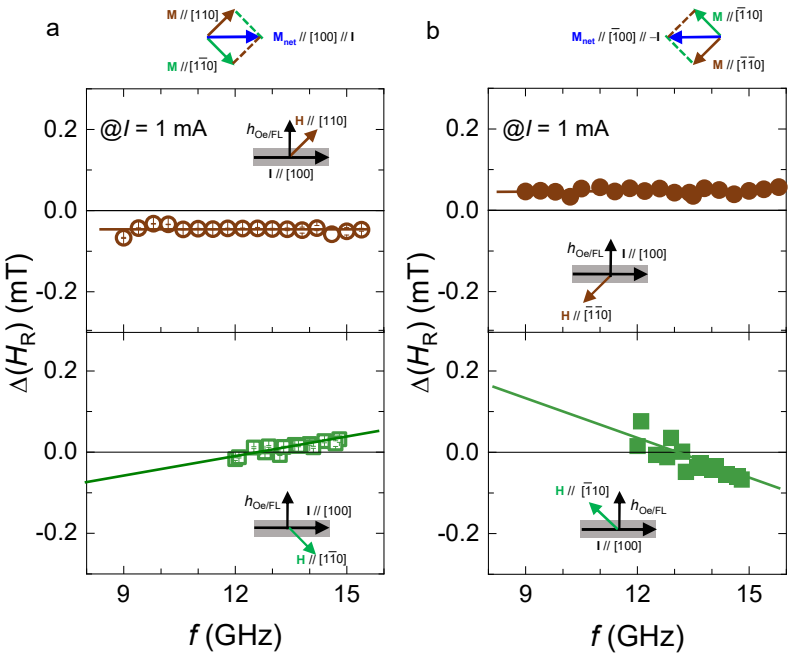


Fig. S11. The same results as Fig. S10 but for $t_{Fe}$ = 2.2 nm.

I) We consider the results obtained for **H** // **M** // [110] (easy axis) and **H** // **M** // [$1\bar{1}0$] (hard axis) as shown in Fig. S10a (the same results as shown in Fig. 4 in the main text for $I$ = 1 mA), where the net magnetization is parallel to **I**. At $f$ = 0, eqs. S17 and 18 are reduced to

$$\Delta H_{\mathrm{R}}^{\mathrm{EA}}(0) = \Delta H_{\mathrm{U}} - \Delta H_{\mathrm{B}} + \frac{\sqrt{2}}{2} h_{\mathrm{Oe/FL}} = -0.20 \text{ mT} \quad \text{(S20)}$$

$$\Delta H_{\mathrm{R}}^{\mathrm{HA}}(0) = -(\Delta H_{\mathrm{U}} + \Delta H_{\mathrm{B}}) - \frac{\sqrt{2}}{2} h_{\mathrm{Oe/FL}} = -0.32 \text{ mT}. \quad \text{(S21)}$$

By adding eqs. S20 and S21, the magnitude of $\Delta H_{\mathrm{B}}$ is determined to be 0.26 mT which corresponds to $k_{\mathrm{B}}$ of $4\times10^{-3}$ mT/GHz according to eq. S17.

II) From Fig. S10a, the slope along the hard axis is determined to be $k_K + k_B = 0.025$ mT/GHz. Thus, the magnitude of $k_{\mathrm{K}}$ is determined by $k_K = 0.025$ mT/GHz$-k_B$ = 0.021 mT/GHz, which corresponds to $\Delta H_{\mathrm{K}}$ = 2.0 mT according to eq. S17.

III) Since $\Delta H_{\mathrm{R}}^{\mathrm{EA}}$ is frequency independent, this requires that $k_U = k_K + k_B = 0.025$ mT/GHz, which corresponds $\Delta H_{\mathrm{U}}$ = 2.5 mT.

Similarly, as the magnetization along EA and HA is respectively rotated by 180° to the [$\bar{1}\bar{1}0$] and [$\bar{1}10$] directions, and the net magnetization is antiparallel to **I** (Fig. S10b), one obtains $\Delta H_{\mathrm{B}}$ = –0.26 mT, $\Delta H_{\mathrm{K}}$ = –2.0 mT and $\Delta H_{\mathrm{U}}$ = –2.5 mT, which are of opposite sign as the results obtained from Fig. S8a. Finally, binging the magnitude of $\Delta H_{\mathrm{B}}$ and $\Delta H_{\mathrm{U}}$ back into eqs. S20 and S21, $\frac{\sqrt{2}}{2} h_{\mathrm{Oe/FL}}$ is determined to be –2.24 mT. The negative sign of $h_{\mathrm{Oe/FL}}$ indicates that it is along [$0\bar{1}0$]-orientation.

Similarly, the corresponding $\Delta H_{\mathrm{B}}$, $\Delta H_{\mathrm{K}}$ and $\Delta H_{\mathrm{U}}$ values can be determined for $t_{\mathrm{Fe}}$ = 2.2 nm (Fig. S11). Table S3 summaries the magnitudes of the magnetic anisotropy modifications as well as the $h_{\mathrm{Oe/FL}}$ values for all the devices. The enhancement of the field-like torque in thinner samples has been

observed in other systems and is probably due to the enhanced Bychkov-Rashba spin-orbit interaction[S15,S16] and/or the orbit angular momentum (orbit Hall effect and orbit Rashba effect) at the ferromagnetic metal/heavy metal interface[S16].

It is worth mentioning that, once the magnetization direction is fixed, $\Delta H_B$, $\Delta H_K$ and $\Delta H_U$ obtained either from Fig. S10a (Fig. S11a) or from Fig. S10b (Fig. S11b) have the same sign (either positive or negative depending on the direction of **M**). This is consistent with the change of magnetic anisotropies by temperature (Figure S12), which shows that the magnitude of $\Delta H_B$, $H_K$ and $\Delta H_U$ increases (decreases) as temperature decreases (increases). This indicates that the increase (decrease) of the magnetic anisotropies is dominated by the increase (decrease) of $M$ as temperature decreases (increases). For the spin current modification case as we demonstrated here, the temperature is not changed but the change of $M$ is induced by populating the electronic bands by the spin current. More interestingly, the new modification method can control the increase or decrease of $M$ simply by the direction of current and/or the direction of magnetization, which is not accessible by other controls.

| | $t_{Fe}$ = 4.5 nm | | $t_{Fe}$ = 2.8 nm | | $t_{Fe}$ = 2.2 nm | | $t_{Fe}$ = 1.2 nm | |
|---|---|---|---|---|---|---|---|---|
| | **+M** | **−M** | **+M** | **−M** | **+M** | **−M** | **+M** | **−M** |
| $\Delta H_B$ (mT) | 0 | 0 | 0 | 0 | 0.11 | −0.138 | 0.26 | −0.26 |
| $\Delta H_K$ (mT) | 0 | 0 | 0 | 0 | 1.5 | −1.8 | 2.0 | −2.0 |
| $\Delta H_U$ (mT) | 0 | 0 | 0 | 0 | 1.6 | −1.9 | 2.5 | −2.5 |
| $\lvert h_{Oe/FL}\rvert$ (mT) | 0.03 | | 0.08 | | 1.56 | | 2.24 | |

Table S3. Summary of $\Delta H_B$, $\Delta H_K$, $\Delta H_U$ and $h_{Oe/FL}$ for $t_{Fe}$ = 4.5 nm, 2.8 nm.2.2 nm and 1.2 nm.

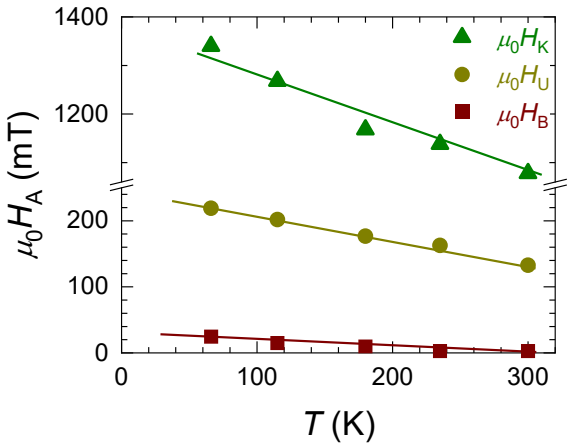


Fig. S12. Temperature dependence of $H_K$, $H_U$ and $H_B$ for $t_{Fe}$ = 1.2 nm.

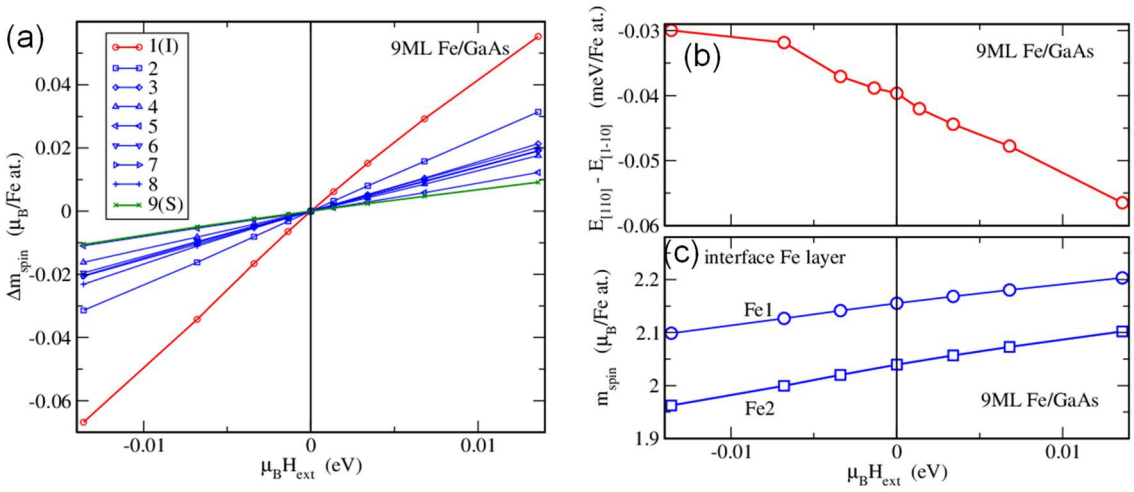


Fig. S13. Calculated results for 9ML Fe films deposited on GaAs(001). (**a**) The layer-resolved change of magnetic moments as a function of applied magnetic field, the 1st layer (I) corresponds to the Fe/GaAs interface, and the 9th layer (S) is the surface layer. (**b**) The energy of the in-plane uniaxial MCA as a function of applied magnetic field. (**c**) Spin magnetic moment of two non-equivalent Fe atoms at the Fe/GaAs interface as a function of the applied magnetic field. Here positive (negative) value corresponds to magnetic field parallel (antiparallel) to the magnetization direction.

## Supplementary Note 7: Theoretical calculation of the modification of magnetic moment and magnetic anisotropy

Experimental measurements on the spin-current-controlled in-plane uniaxial magnetic anisotropy as well as magnetization in ultrathin Fe films on GaAs(001) have been supported by corresponding first principles investigations. We will focus here on the spin-orbit induced magnetic crystalline anisotropy (MCA) contribution only, because of its responsibility for the in-plane uniaxial magnetic anisotropy (UMA) observed in the Fe/GaAs(001) system[S17]. To supply theoretical support to the discussions on the impact of a spin current on the magnetic anisotropy in Fe films on GaAs(001), we are going to use rather simple arguments, which allow to explain the experimental results in terms of the electronic structure. Coming back to the idea represented at the beginning in the main text, we discuss the spin current $\mathbf{J}_S^z$ through the Pt/Al/Fe interface, polarized parallel to the Fe magnetization $\mathbf{m}$ in the case of $\mathbf{m} \,//\, +\mathbf{z}$ , or antiparallel, in the case of $\mathbf{m} \,//\, -\mathbf{z}$. The spin current $\mathbf{J}_S^z$ can be represented in terms of two opposite flows of electrons carrying up and down spin moments, $\mathbf{J}_S^z = \mathbf{J}_{up} - \mathbf{J}_{dw}$, in the absence of a net electric current ($\mathbf{J}_c = \mathbf{J}_{up} + \mathbf{J}_{dw} = 0$). As a consequence, the inflow of the spin-up electrons leads to an increase of occupation of the spin-up d-states of Fe, while the outflow of spin-down electrons leads to a decrease of occupation of the spin-down d-states. Therefore, this leads to an increase of the spin-up electron density $\Delta n_{up}$ and decrease of spin-down electron density $\Delta n_{dw}$, resulting in the change of magnetization $\Delta\mathbf{m}_{tr}$ ($\Delta\mathbf{m}_{tr} = \Delta n_{up} - \Delta n_{dw}$).

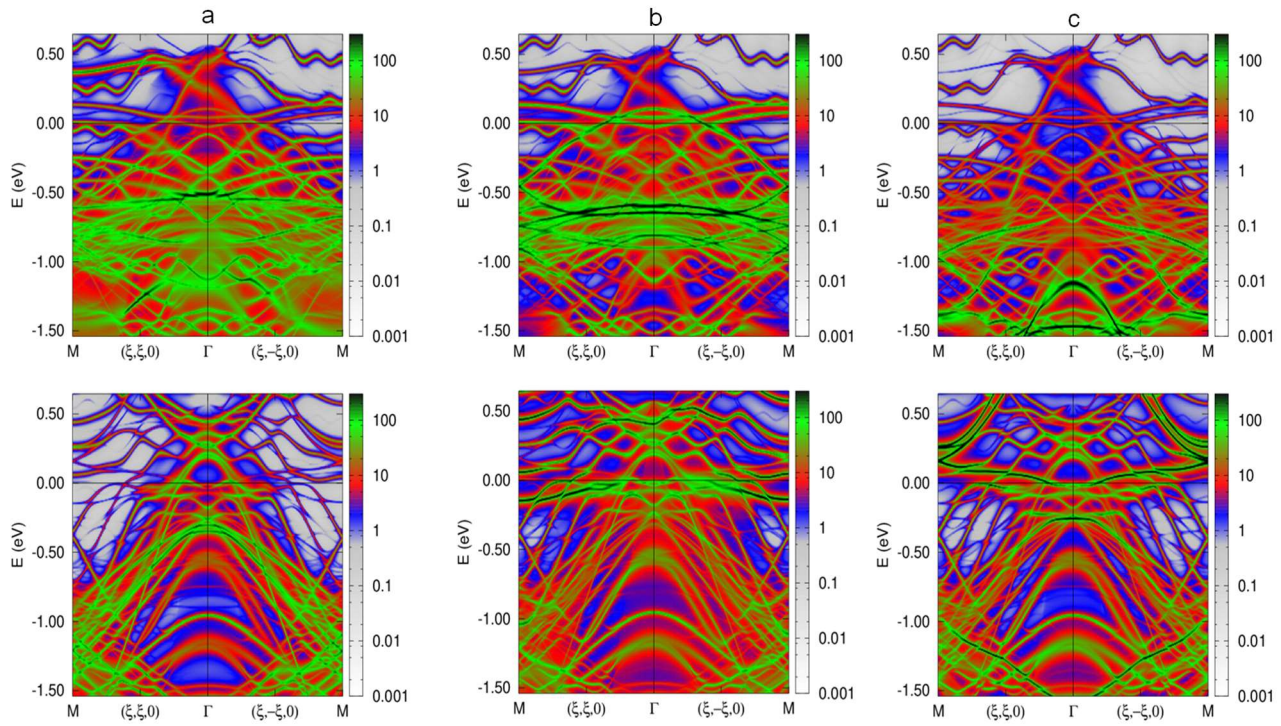


Fig. S14. Layer resolved spin-up (top panel) and spin-down (bottom panel) Bloch spectral function (BSF) for 9ML Fe films deposited on GaAs(001): (**a**) interface Fe layer, (**b**) middle Fe layer, and (**c**) surface Fe layer.

A similar effect occurs in the presence of an applied magnetic field on the scale of molecular field **H** // +**z** shifting the spin-up d-states down in energy, followed by an increase of their occupation, and vice versa, the spin-down d-states shifting up in energy, leading to their depopulation. As a result, the magnetic moments of the Fe atoms increase, if their direction is parallel to the applied field. And decrease of magnetic moment is expected in the case of an antiparallel orientation with respect to the magnetic field. The dependence of the magnetic moment on an applied magnetic field can be studied within first-principles SDFT calculations. Using a varying strength of magnetic field, one can model the impact of the spin current injected into the Fe film on the magnetic properties of the film, depending on the density of the spin current. It should be noted, however, that the strength of the magnetic field used in the calculations is the same for all layers in the Fe film and does not depend

on the distance from the Pt/Fe interface. This is in contrast to the real case that an injected spin current decays in the Fe film with the distance from the interface. Nevertheless, even in the case of a uniform strength of the applied magnetic field, the magnetic response in the Fe film is not trivial, leading to different changes of magnetic moments in the various layers, $\Delta m_i$ (see in Fig. S13(a) the results for 9 MLs of Fe deposited on GaAs(001)). This is, in particular, a consequence of their different spin- and layer-resolved density of states at the Fermi level.

As a next step, we focus on the dependence of the MCA energy on the applied magnetic field, which is used to mimic the effect of an injected spin-current. These calculations are performed for 9 MLs of Fe deposited on GaAs(001) (we consider here the As-terminated interface) (Fig. S13(b)). As the MCA depends on the electronic structure in the vicinity of the Fermi energy, Fig. S14 represents the spin-resolved Bloch spectral function (BSF) $A(E, \mathbf{k})$ within a small energy window around $E_F$, for the wave vector $\mathbf{k}$ along two high-symmetric directions in the 2D Brillouin zone, i.e., $\mathbf{k} = (\xi, \xi, 0)$ and $(\xi, -\xi, 0)$. The intensity of the BSF in Fig. S14 characterize the degree of localization of the electronic states in the interface Fe layer (a), in central layer of the film (b) and at the surface (c), respectively. One can see the obvious difference of the BSF for these two directions. The symmetry of the deposited Fe film is governed by the two-fold symmetry of the GaAs(001) substrate. As one can see that the most distinct asymmetry for the electronic structure along the $(\xi, \xi, 0)$ and $(\xi, -\xi, 0)$ directions is observed for the interface Fe layer due to a strong hybridization of the electronic states of Fe with the states of GaAs. Furthermore, a significant smearing of the energy bands is observed for the interface Fe layer, which are hybridized with bulk-like states of the GaAs substrate. In the middle and surface Fe layers, the smearing of the d-bands, as well as their asymmetry along two BZ directions, decreases. The symmetry properties of the electronic structure determine the symmetry

properties of the magnetic anisotropy, leading to the interfacial origin of uniaxial in-plane MCA.

The MCA energy in this work has been obtained for different values of the applied magnetic field, by means of magnetic torque calculations[S18]. Fig. S13b shows corresponding field-induced changes of the energy of in-plane uniaxial MCA, $E_{UMA} = E_{[110]} - E_{[1\text{-}10]}$. The energy is represented in meV per one Fe atom. As one can see that, in the absence of magnetic field, the easy axis is oriented along the [110] crystallographic direction. The applied magnetic field results in an increase of the MCA energy along the easy axis, $E_{UMA}$, if it is parallel to the magnetization direction, and to a decrease of $E_{UMA}$ in the case of antiparallel orientation. These changes are accompanied by an increase (for $H > 0$) or decrease (for $H < 0$) of the spin magnetic moment of Fe, which is shown in Fig. S13a (the layer-resolved $\Delta m_i$), and in Fig. S13c ( the magnetic moments for the interface Fe atoms).

In order to make a connection of the obtained results with experiment, we represent the magnetic field (shown in Fig. S13 in the units of energy) in terms the spin moment transferred into the Fe film, which was estimated by equating the field induced change of the total spin magnetic moment in the Fe film $\Delta m_{Fe}$ (shown in Fig. S13c) with the spin moment transferred due to a spin current through the interface, $\Delta m_{Fe} = \Delta m_{tr} = \Delta m_{up} - \Delta m_{dw}$. Taking into account the zero electric current ($J_c = 0$) through the interface, one can make a connection between the absolute values of the transferred spin-up density and corresponding change of the magnetization $|\Delta m_{tr}| = 2|\Delta n_{up}|$.

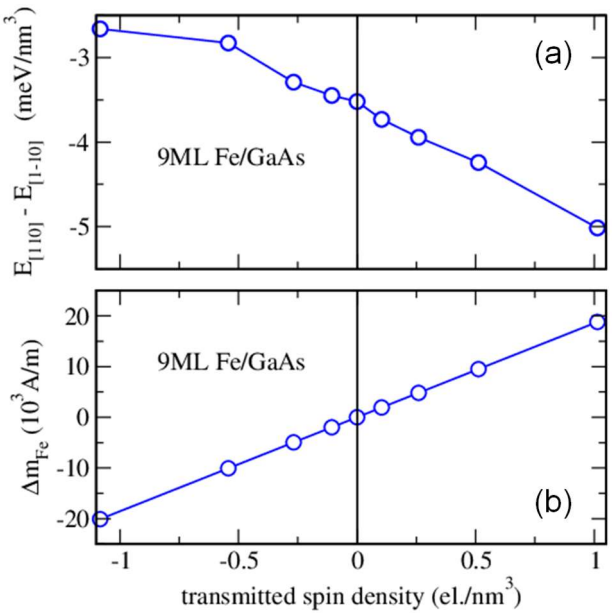


Fig. S15. (**a**) The MCA energy density as a function of the transferred spin density for 9 ML Fe films deposited on GaAs(001). The 'plus' sign corresponds to a transferred spin moment parallel to the magnetization direction, while the 'minus' sign corresponds to the opposite orientation of the transferred spin moment. (**b**) The dependence of the modified magnetization of 9ML Fe films as a function of transferred spin density.

As a result, Fig. S15 replots Fig. S13, which shows the MCA energy density as a function of transferred electron density. By converting the MCA energy density into effective UMA magnetic anisotropy field, one obtains a modulation amplitude of -228 mT/(el./nm$^3$). Considering the experimentally observed $\Delta H_U$ of 2.5 mT, we estimate the number of transferred spin density to be 0.01 el./nm$^3$ (i.e., ~$10^{19}$ cm$^{-3}$). In addition, Fig. S15b shows the dependence of the modified Fe magnetization as a function of the transferred spin density.

Finally, Fig. S16 represents a polar plot for the 9ML Fe/GaAs(001) system, showing the dependence of the MCA energy density, $E(M_{\|}(\varphi)) - E_{[1\text{-}10]}$, on the magnetization angle $\varphi$. The results are obtained for two values of the magnetic field corresponding to a transferred spin density of 1.05

el./nm$^3$ (curve 1) and 1.3 el./nm$^3$ (curve 2), respectively, demonstrating that the impact of the transferred spin moment on the MCA energy density is anisotropic with 2-fold symmetry.

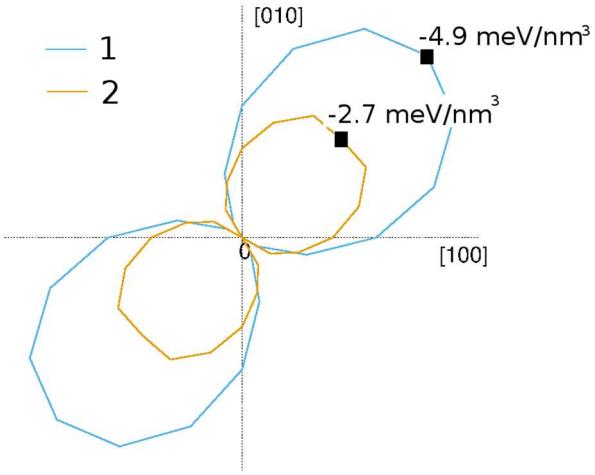


Fig. S16. Results for a 9 ML Fe film deposited on GaAs(001): polar plot for the MCA energy density, $E(M_{||}(\varphi))$ - $E_{[1\text{-}10]}$, as a function of the magnetization angle $\varphi$. Line '1' corresponds to a transferred spin-up electron density of 1.05 el./nm$^3$, and line '2' represents the results for a transferred spin-up electron density of -1.3 el/nm$^3$.

## References

S1. Chen, L., Matsukura, F., & Ohno, H., Direct-current voltages in (Ga,Mn)As structures induced by ferromagnetic resonance. *Nature Commun.* **4**, 2055 (2013).

S2. Chen, L. *et al*. Robust spin-orbit torque and spin-galvanic effect at the Fe/GaAs (001) interface at room temperature. *Nature Commun.* **7**, 13802 (2016).

S3. Chen, L. *et al*. Emergence of anisotropic Gilbert damping in ultrathin Fe layers on GaAs(001). *Nature Phys.* **14**, 490-494 (2018)

S4. Zwierzycki, M. *et al*. First-principles study of magnetization relaxation enhancement and spin transfer in thin magnetic films. *Phys. Rev. B* **71**, 064420 (2005).

S5. Pai, C. F. *et al*. Dependence of efficiency of spin Hall torque on the transparency of Pt/ferromagnetic layer interfaces. *Phys. Rev. B* **92**, 064426 (2015).

S6. Tao, X. *et al*. Self-consistent determination of spin Hall angle and spin diffusion length in Pt and Pd: The role of the interface spin loss. *Sci. Adv.* **4**, eaat1670 (2018).

S7. Xia, K. *et al*. Spin torque in ferromagnetic/normal-metal structures. *Phys. Rev. B* **65**, 220401(R) (2002).

S8. Zhu, L., Ralph, D. C., & Buhrman, R. A., Effective spin-mixing conductance of heavy-metal-ferromagnet interfaces, *Phys. Rev. Lett*. **123**, 057203 (2019).

S9. Manchon, A. *et al*. Current-induced spin-orbit torques in ferromagnetic and antiferromagnetic systems*, Rev. Mod. Phys*. **91**, 035004 (2019).

S10. Kasai, S. *et al*. Modulation of effective damping constant using spin Hall effect, *Appl. Phys. Lett*. **104**, 092408 (2014).

S11. Safranski, C., Montoya, E. A., & Krivorotov, I. N., Spin-orbit torques driven by a planar Hall current, *Nature Nanotech*. **14**, 27-30 (2019).

S12. Capua, A., Rettner, C., & Parkin, S. S. P., Parametric harmonic generation as a probe of unconstrained spin magnetization precession in the shallow barrier limit, *Phys. Rev. Lett*. **116**, 047204 (2016).

S13. Capua, A. *et al*. Phase-resolved detection of the spin Hall angle by optical ferromagnetic resonance in perpendicularly magnetized thin films, *Phys. Rev. B*. **95**, 064401 (2017).

S14. Ando, K. *et al*. Electric manipulation of spin relaxation using spin Hall effect, *Phys. Rev. Lett*. **101**, 036601 (2008).

S15. Chen, L. *et al*. Connection between spin-orbit torques and unidirectional magnetoresistance in ferromagnetic-metal-heavy-metal heterostructures, *Phys. Rev. B*. **105**, L020406 (2022).

S16. Krishnia, S. *et al*. Large interfacial Rashba interaction generating strong spin-orbit torqurs in atomically thin metallic heterostructures, *Nano. Lett*. **23**, 6785-6791 (2023).

S17. Košuth, M. *et al*. Magnetic anisotropy of thin Fe films on GaAs. *Europhys. Lett.* **72**, 816-822 (2005).

S18. Staunton, J. B. *et al*. Temperature dependence of magnetic anisotropy: An *ab initio* approach, *Phys. Rev. B*. **74**, 144411 (2006).